FOURTH-INTEGRAL RESONANCE STUDY ON ALADDIN AT SRC *

J. Liu, E. Crosbie, L. Teng, J. Bridges, D. Ciarlette
APS, Argonne National Laboratory
Argonne, IL 60439, USA

K. Symon
Dept. of Physics, University of Wisconsin-Madison
Madison, WI 53706, USA

W. Trzeciak
Synchrotron Radiation Center, Stoughton, WI 53589, USA

Abstract

The fourth-integral betatron resonance driven by sextupoles was studied on the electron storage ring Aladdin at SRC. The resonance feature of capturing the phase space particles in the resonance islands was clearly demonstrated. In a computer simulation, the finite beam size is simulated by multi-particle tracking and the decoherence of the betatron oscillation was shown to agree well with experiment observation.

1 Introduction

Nonlinear dynamic studies are conducted on the Aladdin electron storage ring at the Synchrotron Radiation Center, University of Wisconsin-Madison. To verify the theoretical prediction of the stability limitation of particle motion, we have experimentally studied the third-order resonances driven by sextupole components of the magnetic field [1], [2], [3]. Our study is now extended to the fourth-order resonance.

*Work supported by U.S. Department of Energy, Office of Basic Energy Sciences under Contract No. W-31-109-ENG-38

The fourth-integral resonance

$$4\nu_x = m \tag{1}$$

can be driven either by the mth harmonic of the first-order effect of the octupole field or by the second-order effect of the sextupole field. The fourth-integral resonance is usually rather weak and does not lead to instabilities. The island feature of the resonance phase map can be obtained relatively easily in the below-resonance case.

The fourth-integral resonance has been observed in the beam experiment in the Aladdin ring by adding an extra sextupole to excite the 29th harmonic. We found that particles captured in the resonance islands did not remain stable in the islands but diffused into the central region due to the quantum fluctuations from photon emission and other stochastic processes.

This report presents the theoretical analysis of the fourth-integral resonance based on Hamiltonian dynamics. The measurement results are presented and compared with computer simulations based on multi-particle tracking. The particle diffusion from the phase-space island in the phase map will be presented in a separate report.

2 Theoretical Analysis

The theoretical analysis is based on Hamiltonian dynamics. We start with the Hamiltonian in terms of action-angle variables γ_x and J_x near a fourth-integral resonance driven by the second-order sextupole effect,

$$H = \nu_x J_x + (2J_x)^2 \epsilon_0 \cos(4\gamma_x - m\theta + \phi_0) + aJ_x^2 \tag{2}$$

where ϵ_0 is a quadratic expression in the sextupole strengths $s \equiv \frac{\beta_x^{3/2}}{48\pi}\frac{B''l}{B\rho}$ and the coefficient a gives the amplitude-dependent tune shift. In addition to quadratic terms in s, a also contains contributions from the quadrupole fringe field and the octupole field. The detailed derivation of this Hamiltonian is given in the Appendix A.

In order to transform away the θ dependence, we take the generating function

$$F(\gamma_x, J; \theta) = J(\gamma_x - \frac{m}{4}\theta + \frac{1}{4}\phi_0) \tag{3}$$

and transform the action-angle variables according to

$$J_x = \frac{\partial F}{\partial \gamma_x} = J, \qquad \gamma = \frac{\partial F}{\partial J} = \gamma_x - \frac{m}{4}\theta + \frac{1}{4}\phi_0. \tag{4}$$

The new Hamiltonian then becomes

$$\mathcal{H} = \epsilon_x J + (2J)^2 \epsilon_0 \cos 4\gamma + aJ^2, \tag{5}$$

where

$$\epsilon_x = \nu_x - \frac{m}{4} \tag{6}$$

is the separation of the tune from the resonant value. The Hamiltonian $\mathcal{H}$ now is a constant of motion. Figure 1 shows the Hamiltonian contours for the case below resonance, i.e. $\epsilon_x < 0$.

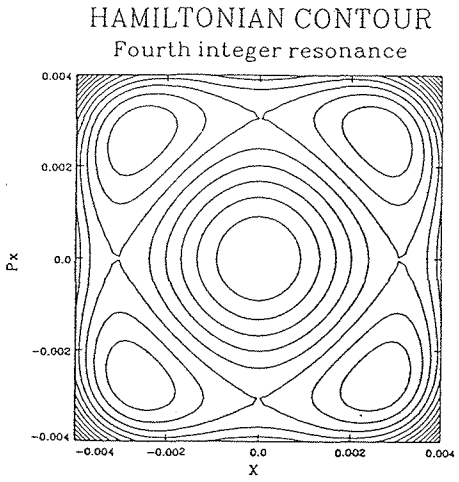

Figure 1: Hamiltonian contour of the fourth-integral resonance at $\epsilon_x = -0.003$ with $\epsilon_0 = 12.563\ m^{-1}$ and $a = 296.527\ m^{-1}$

The resonance is characterized by four islands in the phase space. The fixed points are given by the equations,

$$\frac{\partial \mathcal{H}}{\partial (2J)} = 0, \qquad \frac{\partial \mathcal{H}}{\partial \gamma} = 0\ . \tag{7}$$

The following results are obtained,

$$\gamma = \frac{n\pi}{4}, \qquad (n = 0, 1, 2, 3...),$$
$$(2J)^{1/2} = \left(\frac{|\epsilon_x|}{a + 4\epsilon_0 \cos 4\gamma} \right)^{1/2}. \tag{8}$$

When $\gamma = 0$, $\frac{\pi}{2}$, π, and $\frac{3\pi}{2}$, we have unstable fixed points

$$(2J)_u^{1/2} = \left(\frac{|\epsilon_x|}{a + 4\epsilon_0} \right)^{1/2}, \tag{9}$$

and when $\gamma = \frac{\pi}{4}$, $\frac{3\pi}{4}$, and $\frac{5\pi}{4}$, we get stable fixed points

$$(2J)_s^{1/2} = \left(\frac{|\epsilon_x|}{a - 4\epsilon_0} \right)^{1/2}. \tag{10}$$

The island width is approximately given by

$$W = \left(\frac{|\epsilon_x|}{a-4\epsilon_0}\right)^{1/2} \left\{ \left[1+\left(\frac{8\epsilon_0}{a+4\epsilon_0}\right)^{1/2}\right]^{1/2} - \left[1-\left(\frac{8\epsilon_0}{a+4\epsilon_0}\right)^{1/2}\right]^{1/2} \right\}. \qquad (11)$$

For the case of small ϵ_0, we have

$$W \approx 2\left(\frac{2|\epsilon_x|\epsilon_0}{a^2-16\epsilon_0^2}\right)^{1/2}. \qquad (12)$$

The Hamiltonian analysis describes an isolated nonlinear resonance and yields the basic resonance structure in the phase space.

3 Experiment Measurement

Aladdin is a 1-GeV electron storage ring which is composed of four sectors. The principal parameters of Aladdin are given in Ref [3]. In normal operation, it stores 15 beam bunches with a beam current of 150 mA. For this experiment, only one beam bunch stored at 800 MeV is used and the other 14 bunches are knocked out by the RF knockout technique. One of the spare chromaticity correcting sextupoles is powered to excite the desired resonance. A pulsed-kicker magnet is then fired to kick the beam bunch horizontally to drive a coherent x oscillation. Two pairs of stripline-electrodes measure horizontal displacements of the beam centroid, X_1 and X_2, respectively. Since these two BPMs are separated about 90° in phase, we have approximately $P_{x1} \propto X_2$. If we know the beta functions β_x and the phase advance between locations 1 and 2, the displacements and slopes at location 1 can be precisely calculated. The details of the measurement arrangement as well as data processing are also given in Ref [3] for a previous SRC experiment.

The resonance $4\nu_x = 29$ line is easily accessible. The operating tunes are moved close to the resonance by adjusting the quadrupoles manually. In the measurements, we powered a horizontal focusing sextupole SF10, which is near the beginning of the fourth sector, to a strength of $\frac{B''l}{B\rho} = -6\ m^{-2}$ to excite the 29th harmonic. We took data for 4000 turns after firing the kicker.

Figure 2 shows a typical set of measured data in the BPM units. One BPM unit is $\sim 18.9\ mm$ within a precision of $\pm 10\%$ over a range of 12 mm. The horizontal phase space map P_x versus X is plotted for different kick strength as labelled. The tune was set at $\nu_x = 7.2492$, just below the resonance. Due to the finite beam size, we are actually measuring the motion of the beam centroid. Particles in the beam bunch lose their coherence rather quickly because of the nonlinear tune shift. This makes it difficult to see the explicit resonance feature. The kicker magnet and the BPM X1

are separated about 395° in phase advance. The first phase point is found in the third quadrant in phase plots, which indicates a pinging direction of the pulsed-kicker.

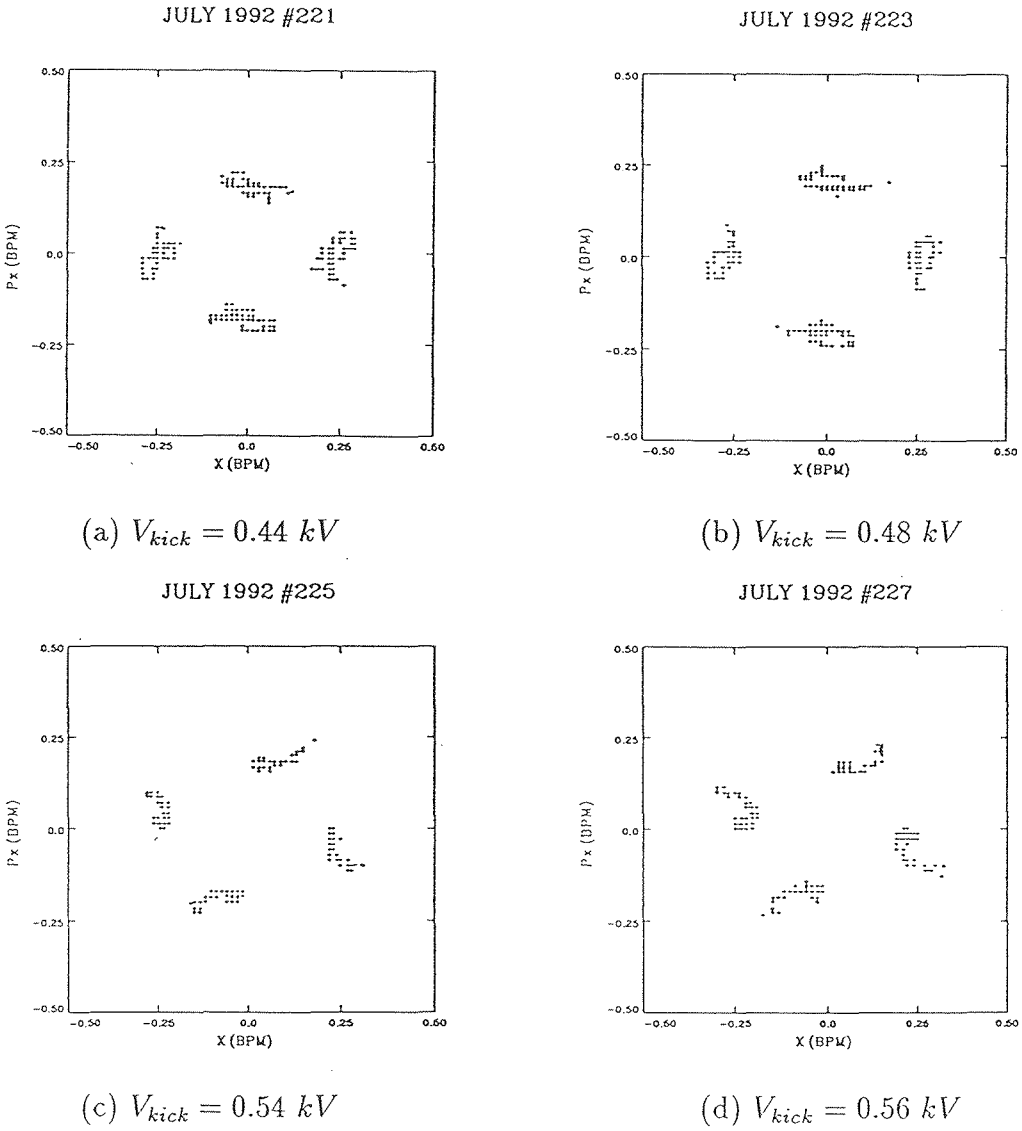

(a) $V_{kick} = 0.44\ kV$

(b) $V_{kick} = 0.48\ kV$

(c) $V_{kick} = 0.54\ kV$

(d) $V_{kick} = 0.56\ kV$

Figure 2: Experimentally measured phase map at $\nu_x = 7.2492$ with sextupole strength $\frac{B''l}{B\rho} = -6.0\ m^{-2}$

Another set of measured data is shown in Figure 3 for the zero-amplitude tune $\nu_x = 7.2485$. When the kick increases from a smaller to a larger value as labelled in the pictures, we obtained different maps. In Figure 3(a) most of the particles were kicked just inside the separatrix; some particles are captured by the resonance island but most were located inside the central stable region. Thus the beam centroid precesses

counter-clockwise initially. Figure 3(b) shows when more particles were kicked into the island. In Figure 3(c) with an even larger kick, most particles were kicked over the island and end up on the outside. Only a small amount were trapped inside the islands. This was somewhat similar to the first case except that the beam centroid initially precesses in the reverse (clockwise) direction. When nearly all the particles were kicked outside of the island, the beam centroid smeared into the central region as shown in Figure 3(d).

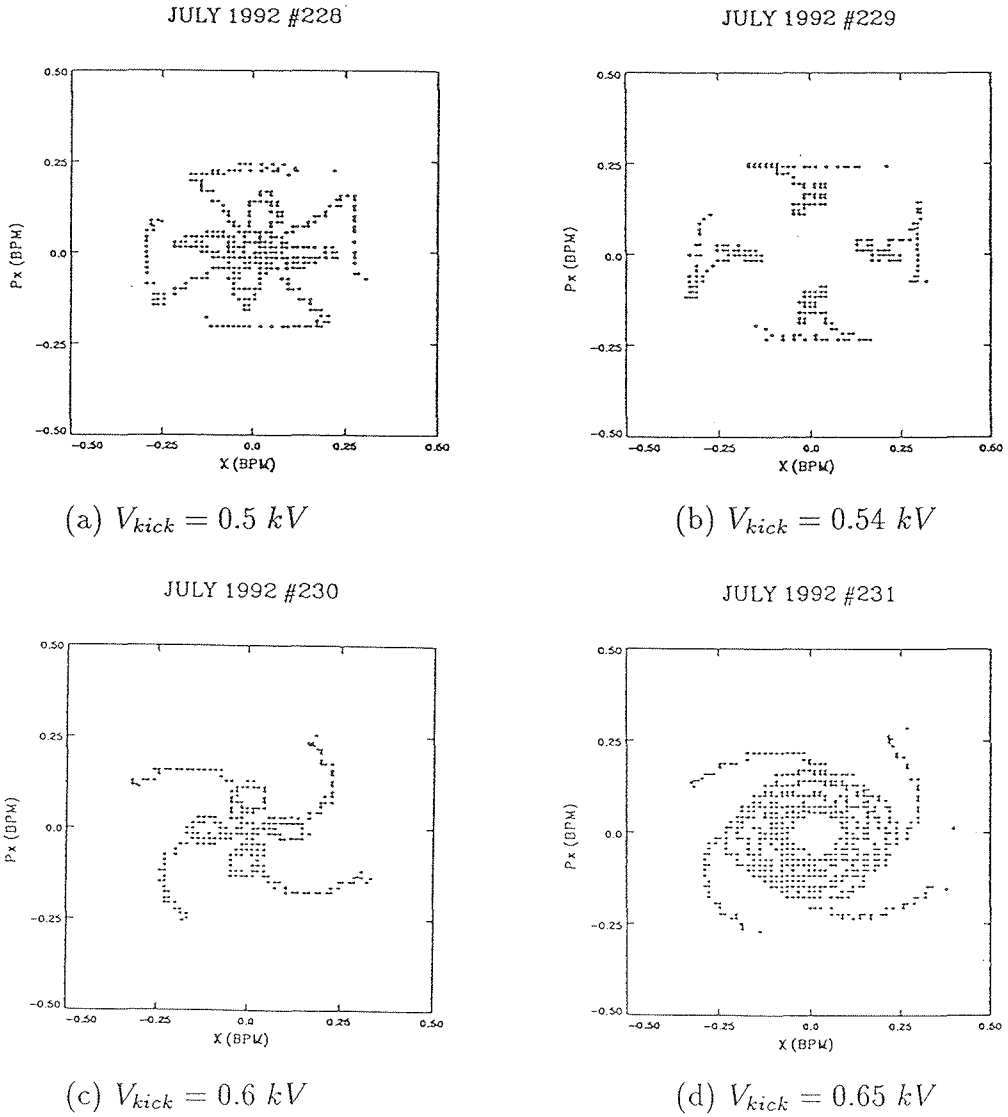

(a) $V_{kick} = 0.5\ kV$

(b) $V_{kick} = 0.54\ kV$

(c) $V_{kick} = 0.6\ kV$

(d) $V_{kick} = 0.65\ kV$

Figure 3: Experimentally measured phase maps at $\nu_x = 7.2485$ with sextupole strength $\frac{B''l}{B\rho} = -6.0\ m^{-2}$

An interesting phenomenon is that phase points move into the center even for

the case where particles were initially captured in the island. Figure 4 is one of the measured sets of data with the same conditions as in Figure 2. We first took data for 4000 turns as shown in Figure 4(a). A half minute later we took data again without kicking beam and we got Figure 4(b). Many repeated measurements showed the same results. It is understood that particles captured in the islands diffuse out slowly and damp toward the origin. This will be studied further in detail at a future experimental run.

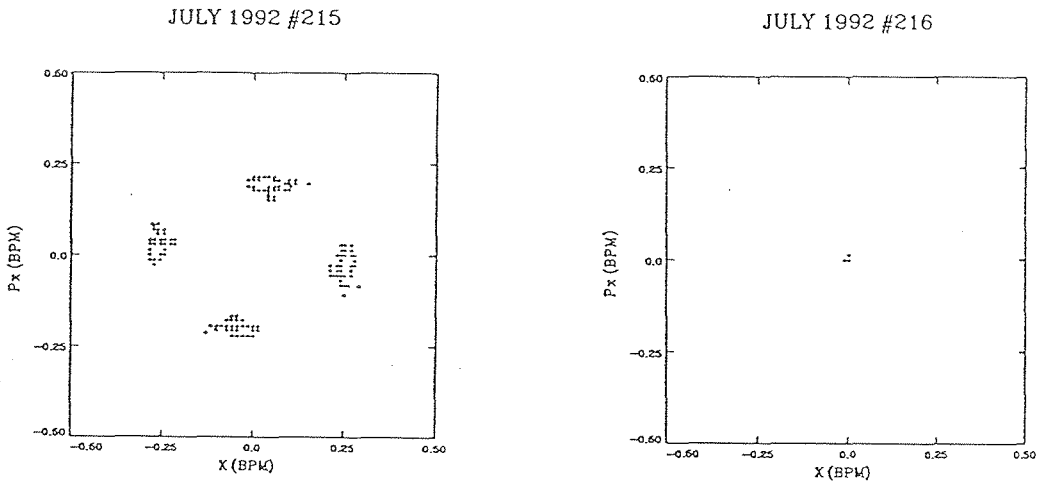

(a) first 4000 turns (b) after a half minute

Figure 4: Resonance island and diffusion

4 Simulation

The numerical tracking of a single particle through the Aladdin lattice confirms the theory presented in Section 2 but does not match exactly the measured results in Figures 3 and 4 because experimental results represent the centroid of the beam bunch containing about 10^{10} electrons which spread out in a sizable area of phase space. Due to the amplitude dependence of the tunes, particles lose their coherence and spread over the phase space in such a way that the beam centroid exhibits an entirely different motion.

A fast tracking code is written to simulate particle behavior under the influence of the nonlinear magnetic force. This code basically uses the following algebraic transformation:

$$\begin{aligned} X_{j+1} &= X_j \cos\phi_{xj} + P_{xj} \sin\phi_{xj} \ , \\ P_{xj+1} &= -X_j \sin\phi_{xj} + P_{xj} \cos\phi_{xj} + \Delta P_{xj} \ , \end{aligned} \tag{13}$$

where $X = x/\sqrt{\beta_x}$ and $P_x = (\beta_x p_x + \alpha_x x)/\sqrt{\beta_x}$. Nonlinear field effects are included in the code as nonlinear kicks ΔP_x given by

$$\Delta P_x = -\sqrt{\beta_x}\frac{\Delta B_x \ell}{B\rho} , \tag{14}$$

where the multipole field ΔB_x is given by

$$\Delta B_x = \sum_n \frac{B^{(n)}}{n!} x^n . \tag{15}$$

Only normal sextupoles and octupoles are included in the code. Using this transformation, one can track the particle motion from one nonlinear element to the next. The lattice parameters are extracted from the program COMFORT.

The driving sextupole strength is set to the same value as the experiment setting. An average octupole field has been added to simulate the contribution of the magnet edge field. It brings the amplitude-dependent tune shift into agreement with the observed value. Since we only calculate 4000 turns, the quantum fluctuation excitation and RF acceleration damping do not contribute and hence they are not included.

To simulate the beam, 100 particles are tracked and the centoid motion of the particles is plotted in the phase space map. Initially the beam is represented by a Gaussian distribution in the X and P_x phase space with $\sigma_x = 0.82\ mm$, which is generated by a random number generator. The coordinates of the centroid are calculated after each turn.

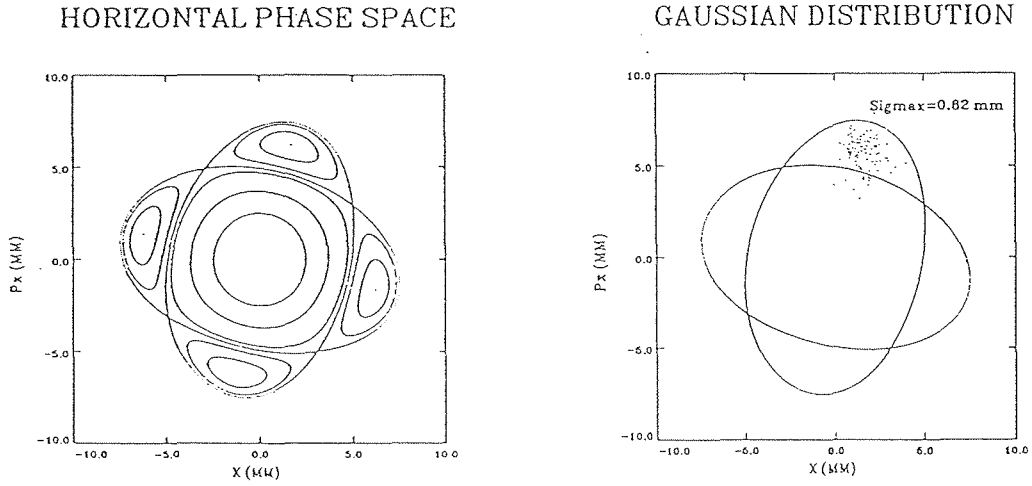

(a) Resonance phase map

(b) Initial particle distribution

Figure 5: Illustration at $\nu_x = 7.2485$ with sextupole strength $\frac{B''l}{B\rho} = -6.0\ m^{-2}$ and octupole strength $\frac{B'''l}{B\rho} = -300.0\ m^{-2}$

Figure 5 (a) shows a single particle tracking. Several phase trajectories are plotted together. Figure 5 (b) illustrates a Gaussian distributed beam when it is kicked into an island. Due to the finite beam size, some particles are located outside the island.

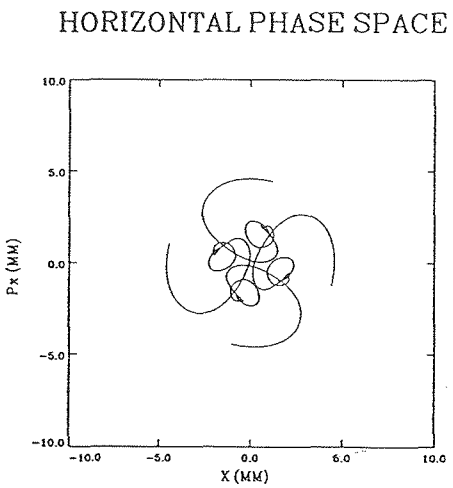

(a) $X_0 = 1.29\ mm$, $P_{x0} = 4.34\ mm$

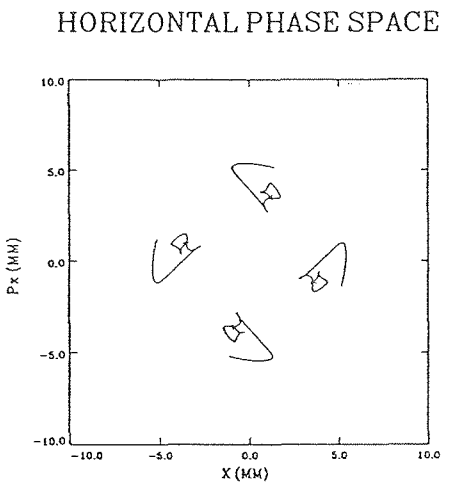

(b) $X_0 = 1.44\ mm$, $P_{x0} = 5.18\ mm$

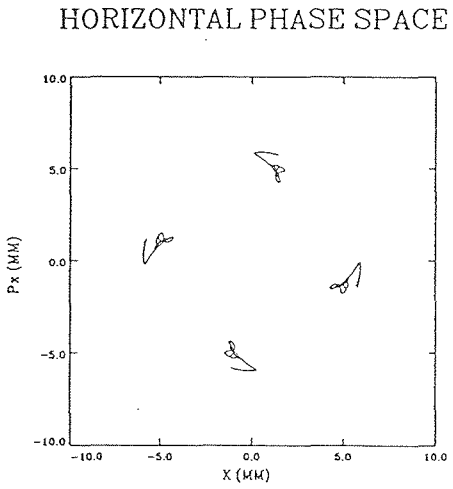

(c) $X_0 = 1.71\ mm$, $P_{x0} = 6.05\ mm$

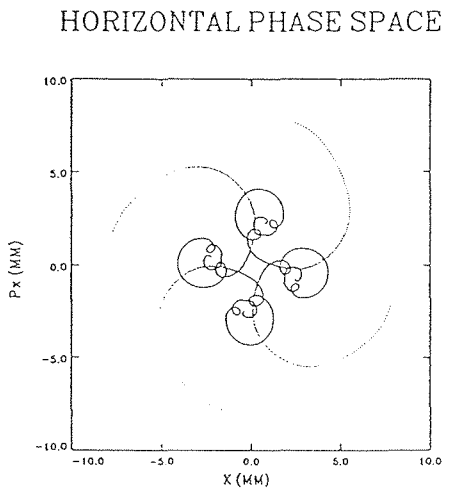

(d) $X_0 = 2.12\ mm$, $P_{x0} = 7.65\ mm$

Figure 6: Simulation results for 100 particles at $\nu_x = 7.2485$ with sextupole strength $\frac{B''l}{B\rho} = -6.0\ m^{-2}$ and octupole strength $\frac{B'''l}{B\rho} = 300\ m^{-3}$

Figure 6 shows several phase plots of beam centoid motion with different initial values as labelled on each plot. The first plot corresponds to Figure 3 (a) with most particles initially located inside the central stable region; the second plot is similar to Figure 3 (b) in which most particles are kicked into the island. In the third plot the

beam is kicked close to the island stable point and the last plot corresponds to Figure 3 (d) with most particles over kicked outside the island. Due to the decoherence, the oscillatory beam centoid motion eventually damps to four stable spots in the phase space. Beware that those four spots are not the fixed stable points as defined in Section 2. As we see in Figure 6, the beam trajectories in the phase space are in agreement with the measurements and show all the observed features with roughly correct magnitudes.

5 Conclusion

We have measured the motion of the electron beam near the fourth-integral resonance $4\nu_x = 29$ in the Aladdin ring under the second-order effect of the driving sextupole. The general features of the single particle dynamics are semi-quantitatively confirmed by the measurement. Exact agreement between analysis and measurement is difficult because of the unknown errors in the ring and the large beam emittance. Computer simulation using multi-particle tracking shows a good agreement with measurements and thus confirms the validity of the analytical and numerical treatments of the nonlinear motion near the fourth-integral resonance.

The measurements also show that the radiation damping and excitation effects are important factors in the 1 minute time scale near the fourth-integral resonance. These and other stochastic effects cause the particles to diffuse out of the stable islands into the central stable region. A further experiment is being planned to study this phenomenon in detail.

References

[1] J. Bridges, *et al., Particle Accelerators*, **28**, 1 (1990)

[2] E. Crosbie, *et al.*, IEEE Particle Accelerator Conference, 91CH3038-7, Vol. 3 (1991)

[3] J. Liu, *et al.*, "Difference Resonance Study on the Electron Storage Ring ALADDIN at SRC," LS-183, ANL Report, 1991

Appendix A Hamiltonian Formalism

The Hamiltonian treatment for the fourth-integral resonance driven by sextupoles is presented below for reference.

After the Floquet transformation, the Fourier expansion, and the Moser transformation, we obtain the Hamiltonian in the following form

$$\begin{aligned} H &= \nu_x J_x + 12 J_x^2 \sum_n [A_{3n} \cos q_{3n} + 3A_{1n} \cos q_{1n}] \\ &\quad \times \sum_{n'} \left[\frac{3A_{3n'}}{n' - 3\nu_x} \cos q_{3n'} + \frac{3A_{1n'}}{n' - \nu_x} \cos q_{1n'} \right], \end{aligned} \tag{A1}$$

where γ_x and J_x are action-angle variables, and

$$\begin{aligned} q_{3n} &= 3\gamma_x - n\theta + \alpha_{3n} \\ q_{1n} &= \gamma_x - n\theta + \alpha_{1n} \\ A_{3n} e^{i\alpha_{3n}} &= \sum_j s_j e^{i(3\psi_x - 3\nu_x + n\theta)_j}, \\ A_{1n} e^{i\alpha_{1n}} &= \sum_j s_j e^{i(\psi_x - \nu_x + n\theta)_j}, \\ s_j &= \left(\frac{B'' l \beta_x^{3/2}}{48\pi B\rho} \right)_j, \end{aligned} \tag{A2}$$

and $\theta = \frac{s}{R}$, n is the circumferential harmonic number, and $\frac{B'' l}{B\rho}$ is the sextupole strength. The above equation can be rewritten as

$$\begin{aligned} H &= \nu_x J_x + 18 J_x^2 \sum_{n,n'} \left[\frac{A_{3n} A_{3n'}}{n' - 3\nu_x} \cos Q_1 + \frac{A_{3n} A_{3n'}}{n' - 3\nu_x} \cos Q_{10} + \frac{3A_{1n} A_{1n'}}{n' - \nu_x} \cos Q_2 \right. \\ &\quad + \frac{3A_{1n} A_{1n'}}{n' - \nu_x} \cos Q_{20} + \frac{A_{3n} A_{1n'}}{n' - \nu_x} \cos Q_3 + \frac{A_{3n} A_{1n'}}{n' - \nu_x} \cos Q_4 \\ &\quad \left. + \frac{3A_{1n} A_{3n'}}{n' - 3\nu_x} \cos Q_5 + \frac{3A_{1n} A_{3n'}}{n' - 3\nu_x} \cos Q_6 \right], \end{aligned} \tag{A3}$$

where

$$\begin{aligned} Q_1 &= 6\gamma_x - (n + n')\theta + (\alpha_{3n} + \alpha_{3n'}), \\ Q_{10} &= -(n - n')\theta + (\alpha_{3n} - \alpha_{3n'}), \\ Q_2 &= 2\gamma_x - (n + n')\theta + (\alpha_{1n} + \alpha_{1n'}), \\ Q_{20} &= -(n - n')\theta + (\alpha_{1n} - \alpha_{1n'}), \\ Q_3 &= 4\gamma_x - (n + n')\theta + (\alpha_{3n} + \alpha_{1n'}), \\ Q_4 &= 2\gamma_x - (n - n')\theta + (\alpha_{3n} - \alpha_{1n'}), \\ Q_5 &= 4\gamma_x - (n + n')\theta + (\alpha_{3n'} + \alpha_{1n}), \\ Q_6 &= 2\gamma_x - (n - n')\theta + (\alpha_{3n'} - \alpha_{1n}). \end{aligned} \tag{A4}$$

To remove those non-dominant terms, we assume a generating function

$$\begin{aligned} G(\gamma_x, \underline{J}_x; \theta) &= \gamma_x \underline{J}_x + 18\underline{J}_x^2 \sum_{n,n'} [G_{1n} \sin Q_1 + G_{2n} \sin Q_2 + G_{3n} \sin Q_3 \\ &\quad + G_{4n} \sin Q_4 + G_{5n} \sin Q_5 + G_{6n} \sin Q_6] \\ &\quad + 18\underline{J}_x^2 \sum_{\substack{n,n' \\ n \neq n'}} [G_{10n} \sin Q_{10} + G_{20n} \sin Q_{20}], \end{aligned} \tag{A5}$$

where parameters G_{qn} are adjusted to make the non-dominant terms vanish. From the generating function, we obtain new variables $\underline{\gamma}_x$, $\underline{J}_x$ given by

$$\begin{aligned} J_x &= \frac{\partial G}{\partial \gamma_x} = \underline{J}_x + 18\underline{J}_x^2 \sum_{n,n'} [6G_{1n} \cos Q_1 + 2G_{2n} \cos Q_2 \\ &\quad + 4G_{3n} \cos Q_3 + 2G_{4n} \cos Q_4 + 4G_{5n} \cos Q_5 + 2G_{6n} \cos Q_6], \\ \underline{\gamma}_x &= \frac{\partial G}{\partial \underline{J}_x} = \gamma_x + 36\underline{J}_x \sum_{n,n'} [G_{1n} \sin Q_1 + G_{2n} \sin Q_2 + G_{3n} \sin Q_3 \\ &\quad + G_{4n} \sin Q_4 + G_{5n} \sin Q_5 + G_{6n} \sin Q_6] \\ &\quad + 36\underline{J}_x \sum_{\substack{n,n' \\ n \neq n'}} [G_{10n} \sin Q_{10} + G_{2n0} \sin Q_{20}], \end{aligned} \tag{A6}$$

and

$$\begin{aligned} \frac{\partial G}{\partial \theta} &= 18\underline{J}_x^2 \sum_{n,n'} [-(n+n')G_{1n} \cos Q_1 - (n+n')G_{2n} \cos Q_2 \\ &\quad - (n+n')G_{3n} \cos Q_3 - (n-n')G_{4n} \cos Q_4 - (n'+n)G_{5n} \cos Q_5 \\ &\quad - (n'-n)G_{6n} \cos Q_6] + 18\underline{J}_x^2 \sum_{\substack{n,n' \\ n \neq n'}} [-(n-n')G_{10n} \cos Q_{10} \\ &\quad - (n-n')G_{20n} \cos Q_{20}]. \end{aligned} \tag{A7}$$

The new Hamiltonian has the form

$$\begin{aligned} \mathcal{H} &= \nu_x \underline{J}_x + 18\underline{J}_x^2 \sum_{n,n'} \left\{ \left[\frac{A_{3n} A_{3n'}}{n' - 3\nu_x} - ((n+n') - 6\nu_x) G_{1n} \right] \cos Q_1 \right. \\ &\quad + \left[\frac{3A_{1n} A_{1n'}}{n' - \nu_x} - ((n+n') - 2\nu_x) G_{2n} \right] \cos Q_2 \\ &\quad + \left[\frac{A_{3n} A_{1n'}}{n' - \nu_x} - ((n+n') - 4\nu_x) G_{3n} \right] \cos Q_3 \\ &\quad + \left[\frac{A_{3n} A_{1n'}}{n' - \nu_x} - ((n-n') - 2\nu_x) G_{4n} \right] \cos Q_4 \\ &\quad + \left[\frac{3A_{1n} A_{3n'}}{n' - 3\nu_x} - ((n+n') - 4\nu_x) G_{5n} \right] \cos Q_5 \end{aligned}$$

$$+\left[\frac{3A_{1n}A_{3n'}}{n'-3\nu_x}-((n'-n)-2\nu_x)G_{6n}\right]\cos Q_6\Big\}$$
$$+18\underline{J}_x^2\sum_n\left[\frac{A_{3n}^2}{n-3\nu_x}+\frac{3A_{1n}^2}{n-\nu_x}\right]. \tag{A8}$$

In this general Hamiltonian, we are only interested in those terms related to the fourth-integral resonance. To make the non-dominant terms vanish, we set

$$\begin{aligned}
G_{1n} &= \frac{A_{3n}A_{3n'}}{(n-3\nu_x)[(n+n')-6\nu_x]},\\
G_{10n} &= \frac{A_{3n}A_{3n'}}{(n-3\nu_x)(n+n')},\\
G_{2n} &= \frac{3A_{1n}A_{1n'}}{(n-\nu_x)[(n+n')-2\nu_x]},\\
G_{20n} &= \frac{3A_{1n}A_{1n'}}{(n-\nu_x)(n+n')},\\
G_{4n} &= \frac{A_{3n}A_{1n'}}{(n-3\nu_x)[(n-n')-2\nu_x]},\\
G_{6n} &= \frac{3A_{1n}A_{3n'}}{(n-3\nu_x)[(n-n')-2\nu_x]},
\end{aligned} \tag{A9}$$

and

$$G_{3n}=0, \quad G_{5n}=0. \tag{A10}$$

The explicit expression of the Hamiltonian for the fourth-integral resonance can now be written as

$$\begin{aligned}
\mathcal{H} &= \nu_x\underline{J}_x+18\underline{J}_x^2\sum_{n,n'}\left[\frac{A_{3n}A_{1n'}}{n'-\nu_x}\cos Q_3+\frac{3A_{1n}A_{3n'}}{n'-3\nu_x}\cos Q_5\right]\\
&\quad +18\underline{J}_x^2\sum_n\left[\frac{A_{3n}^2}{n-3\nu_x}+\frac{3A_{1n}^2}{n-\nu_x}\right].
\end{aligned} \tag{A11}$$

Using Eq. (A2) and the constraint of $n+n'=m$ (resonance harmonic), we can write the second term of the above equation as

$$\begin{aligned}
(2nd\ term) &= 18\underline{J}_x^2 Re\left\{\sum_{j1,j2}s_{j1}s_{j2}\sum_{n'}\left[\frac{e^{i[3\psi_{xj1}+\psi_{xj2}-3\nu_x\theta_{j1}-\nu_x\theta_{j2}+m\theta_{j1}+n'(\theta_{j2}-\theta_{j1})]}}{n'-\nu_x}\right.\right.\\
&\quad \left.\left.+\frac{3e^{i[3\psi_{xj1}+\psi_{xj2}-3\nu_x\theta_{j1}-\nu_x\theta_{j2}+m\theta_{j2}+n'(\theta_{j1}-\theta_{j2})]}}{n'-3\nu_x}\right]e^{i(4\gamma_x-m\theta)}\right\}.
\end{aligned} \tag{A12}$$

To simplify the expression, we use the following equality,

$$\sum_{n=-\infty}^{\infty}\frac{e^{i(n\theta+b)}}{n-\nu}=\begin{cases}-\frac{\pi}{\sin\pi\nu}e^{i[b+\nu(\theta-\pi)]}, & 0<\theta<2\pi\\ -\pi\cot\pi\nu\ e^{ib}, & \theta=0.\end{cases} \tag{A13}$$

Thus we have

$$(2nd\ term) = 18\underline{J}_x^2 Re\left\{\sum_{j1,j2} s_{j1}s_{j2}\left[-\frac{\pi}{\sin\pi\nu_x}e^{i(4\gamma_x - m\theta+\delta_1)} - \frac{3\pi}{\sin 3\pi\nu_x}e^{i(4\gamma_x-m\theta+\delta_2)}\right]\right\}, \tag{A14}$$

where

$$\begin{aligned}\delta_1 &= 3\psi_{xj1} + \psi_{xj2} - 4\epsilon_x\theta_{j1} - \pi\nu_x,\\ \delta_2 &= 3\psi_{xj1} + \psi_{xj2} - 4\epsilon_x\theta_{j2} - 3\pi\nu_x.\end{aligned} \tag{A15}$$

A little more algebraic work leads finally to the Hamiltonian given in Eq. (2),

$$\mathcal{H} = \nu_x\underline{J}_x + (2\underline{J}_x)^2\epsilon_0\cos(4\gamma_x - m\theta + \phi_0) + a\underline{J}_x^2 \tag{A16}$$

where

$$\begin{aligned}\epsilon_0 &= \sqrt{\epsilon_1^2+\epsilon_2^2},\\ \phi_0 &= tan^{-1}\frac{\epsilon_2}{\epsilon_1},\\ \epsilon_1 &= -\frac{9}{2}\sum_{j1,j2} s_{j1}s_{j2}\left(\frac{\pi\sin\delta_1}{\sin\pi\nu_x} + \frac{3\pi\sin\delta_2}{\sin 3\pi\nu_x}\right),\\ \epsilon_2 &= -\frac{9}{2}\sum_{j1,j2} s_{j1}s_{j2}\left(\frac{\pi\cos\delta_1}{\sin\pi\nu_x} + \frac{3\pi\cos\delta_2}{\sin 3\pi\nu_x}\right),\end{aligned} \tag{A17}$$

and

$$a = 18\sum_n\left[\frac{A_{3n}^2}{n-3\nu_x} + \frac{3A_{1n}^2}{n-\nu_x}\right]. \tag{A18}$$